BioOne COMPLETE

RSM-BBD Optimization of Fenton-Like Degradation of 4-Nitrophenol Using Magnetite Impregnated Kaolin

Authors: Belachew, Neway, Fekadu, Redeat, and Ayalew Abebe, Amare

Source: Air, Soil and Water Research, 13(1)

Published By: SAGE Publishing

URL: https://doi.org/10.1177/1178622120932124

BioOne Complete (complete.BioOne.org) is a full-text database of 200 subscribed and open-access titles in the biological, ecological, and environmental sciences published by nonprofit societies, associations, museums, institutions, and presses.

Your use of this PDF, the BioOne Complete website, and all posted and associated content indicates your acceptance of BioOne's Terms of Use, available at www.bioone.org/terms-of-use.

Usage of BioOne Complete content is strictly limited to personal, educational, and non - commercial use. Commercial inquiries or rights and permissions requests should be directed to the individual publisher as copyright holder.

BioOne sees sustainable scholarly publishing as an inherently collaborative enterprise connecting authors, nonprofit publishers, academic institutions, research libraries, and research funders in the common goal of maximizing access to critical research.

Downloaded From: https://complete.bioone.org/journals/Air,-Soil-and-Water-Research on 28 Mar 2024
Terms of Use: https://complete.bioone.org/terms-of-use

RSM-BBD Optimization of Fenton-Like Degradation of 4-Nitrophenol Using Magnetite Impregnated Kaolin

Neway Belachew, Redeat Fekadu and Amare Ayalew Abebe

Department of Chemistry, Debre Berhan University, Debre Berhan, Ethiopia.

Air, Soil and Water Research
Volume 13: 1–10
© The Author(s) 2020
Article reuse guidelines:
sagepub.com/journals-permissions
DOI: 10.1177/1178622120932124

SAGE

ABSTRACT: In this work, we have reported a low-cost and environmentally friendly Fe_3O_4-modified activated kaolin (AK-Fe_3O_4) composite for efficient Fenton-like degradation of 4-nitrophenol (4-NP) and optimization of the degradation variables. The AK-Fe_3O_4 composites were characterized by Fourier transform infrared spectroscopy, powder x-ray diffraction, scanning electron microscopy (SEM), and vibrating sample magnetometer (VSM). X-ray diffraction confirms the syntheses of pure phases of Fe_3O_4 and AK-Fe_3O_4. The SEM image of the AK-Fe_3O_4 composite reveals the formation of a highly porous surface. The room temperature VSM analysis describes the superparamagnetic nature of AK-Fe_3O_4 composites with 25 emu/g magnetization values. Response surface methodology coupled with Box-Behnken design was used to optimize the 4-NP degradation (%) variables such as contact time (10-90 minutes), 4-NP concentration (10-30 mg/L), and pH (3-8). The high regression value ($R^2 = 0.9964$ and adjusted $R^2 = 0.9917$) and analysis of variance ($P < .0001$) show that the quadratic model can sufficiently explain the 4-NP degradation (%). The optimum 4-NP degradation was found to be 96.01% ± 1.89% using 1 mg/mL of AK-Fe_3O_4, 20 mg/L of 4-NP, 97.9 mmol/L of H_2O_2, and pH of 3 at the end of 75 minutes of reaction time. Moreover, the catalyst shows good recyclability and stability after 5 successive degradations of 4-NP. In general, a low-cost and magnetically separable AK-Fe_3O_4 composite is an effective Fenton-like catalyst for the degradation of 4-NP.

KEYWORDS: Kaolin, Fe_3O_4, 4-nitrophenol, Fenton-like degradation, ANOVA

RECEIVED: May 4, 2020. **ACCEPTED:** May 13, 2020.

TYPE: Original Research

FUNDING: The author(s) received no financial support for the research, authorship, and/or publication of this article.

DECLARATION OF CONFLICTING INTERESTS: The author(s) declared no potential conflicts of interest with respect to the research, authorship, and/or publication of this article.

CORRESPONDING AUTHOR: Neway Belachew, Department of Chemistry, Debre Berhan University, P.O. Box. 445, Debre Berhan, Ethiopia. Email: neway.du@gmail.com

Introduction

The unwarranted release of toxic effluents from domestic sewage, agricultural wastewater, and industrial wastes adversely contaminates the water bodies. Currently, wastewater discharge from industries such as textile, leather, cosmetics, plastics, pharmaceuticals, pesticides, food processing, and papers composed of numerous organic and inorganic water contaminants shows antagonistic effects in the water quality.[1,2] More importantly, colored organic compounds discharged into water bodies prevent the penetration of sunlight which affects the photosynthesis process in the aquatic environment.[3] Moreover, such organic compounds are also toxic to humans and animals. 4-nitrophenol (4-NP) is a nitroaromatic compound, widely used as a precursor for the preparation of pharmaceutics and pesticides. Conversely, 4-NP is one of the hazardous chemicals affecting both human and animal health.[4,5] The Agency for Toxic Substances and Disease Registry (ATSDR) of the United States designated 4-NP as one of the 114 organic compounds listed, which poses a great danger to living organisms in the environment.[6] Hence, 4-NP needs to be removed from wastewater before being discharged into the environment. There are various physical, chemical, and biological treatments such as photocatalytic degradation,[7] flocculation,[8] ion exchange,[9] membrane filtration,[10] adsorption,[11] and Fenton-like degradation[12] that have been investigated to remove these contaminants from wastewater. 4-nitrophenol owing to its extreme stability is unable to be easily removed from aqueous solutions using conventional approaches. There is considerable interest in Fenton-like technology due to low cost, simple procedures, and mild operating conditions for the degradation of organic pollutants.[13] Fenton-like is an advanced oxidation process (AOP) that has tremendous potential for the degradation of a broad range of organic compounds. The hydroxyl radical ($HO^{\bullet}$) generated in AOPs has strong redox potential (2.80 eV) and can react with almost all stable organic compounds.[14] The conventional Fenton process (Fe^{2+}/H_2O_2) owing to working in an extremely acid solution (pH <4) and due to the formation of ferric hydroxide sludge during wastewater treatment is not suitable for practical applications.[15,16] Hence, an alternative Fenton-like catalyst substitute Fe^{2+}/H_2O_2 is desirable to overcome the aforementioned problems.

Recently, heterogeneous Fenton-like catalysts have been reported as an alternative for the efficient degradation of recalcitrant organic compounds. Fenton catalysts such as $CuFe_2O_4$,[17] α-FeOOH,[18] Fe_2O_3/Al_2O_3,[19] and Fe_3O_4[20] have been widely used in combination with H_2O_2 for the formation of reactive $HO^{\bullet}$ radicals. In particular, Fe_3O_4 has received considerable attention in water treatment due to its excellent chemical stability, biocompatibility, and high magnetic saturation value.[21] However, Fe_3O_4 nanoparticles due to their strong magnetic dipole-dipole interaction and large surface area are vulnerable to irreversible agglomeration, which in turn decreases the efficiency. The irreversible agglomeration of Fe_3O_4 nanoparticles (NPs) can be prevented by immobilization on different supporting materials such as metal-organic framework, graphene oxide, reduced graphene oxide, amino acids, polymer, cellulose, chitosan, and clay minerals.[22,23] A low-cost and naturally abundant kaolin clay due to high surface porosity shows excellent

Creative Commons Non Commercial CC BY-NC: This article is distributed under the terms of the Creative Commons Attribution-NonCommercial 4.0 License (https://creativecommons.org/licenses/by-nc/4.0/) which permits non-commercial use, reproduction and distribution of the work without further permission provided the original work is attributed as specified on the SAGE and Open Access pages (https://us.sagepub.com/en-us/nam/open-access-at-sage).

Downloaded From: https://complete.bioone.org/journals/Air,-Soil-and-Water-Research on 28 Mar 2024
Terms of Use: https://complete.bioone.org/terms-of-use

efficiency for adsorption of various guest materials including inorganic metal oxides.[24] Besides, kaolin can be used as a supporting material for various metal oxides to enhance their catalytic performances. For example, Guo et al[25] have reported an enhanced photo-Fenton degradation of rhodamine B by kaolin-Fe_2O_3 than Fe_2O_3 NPs. Similarly, Giri et al[26] reported a high-surface-area kaolin-supported Fe_3O_4 adsorbent for the removal of water pollutants. Kaolin-ZnO NPs and kaolin-TiO_2 NPs are also reported as efficient photocatalysts for the degradation of organic compounds.[27,28] Ayodele and Hameed also reported kaolinite-supported ferric oxalate for photo-Fenton degradation of 4-NP.[29] But there is no report on use of kaolin-Fe_3O_4 for Fenton-like degradation of 4-NP and detailed process optimizations.

Moreover, the efficiency of Fenton-like AOPs is varied with the interaction of different process parameters, such as contact time, pH of the solution, catalyst dose, and concentration of the substrate. Therefore, optimization of process variables using a systematic approach which requires fewer experiments and shows the interaction of process variables is highly desirable for practical application. The conventional optimization approaches are time-consuming, require a large number of runs, and are not able to clearly show the interaction of process variables.[30] The response surface methodology (RSM) has been widely applied to optimize and investigate the interaction of different variables during the experiment.[31,32] The RSM can effectively optimize experimental variables using a small number of experiments within a short period of time.[30] The RSM based on Box-Behnken design (BBD) optimization is the most recommended design approach for a 3-level incomplete factorial design. The BBD requires fewer experiments and estimates the factors in a quadratic model, which contains squared terms, products of 2 factors, linear terms, and an intercept.[33]

Herein, we have reported a detailed RSM-BBD optimization of the Fenton-like degradation of 4-NP using kaolin-Fe_3O_4 composites. One-pot synthesis of Fe_3O_4 NPs in kaolin was used for the preparation of the composite. Powder x-ray diffraction (XRD), Fourier transform infrared spectroscopy (FTIR), scanning electron microscopy (SEM), and vibrating sample magnetometer (VSM) techniques were used to investigate phase, functional group, morphology, and magnetic properties of the composite, respectively. The Fenton-like degradation process was optimized using RSM-BBD at various contact time (minutes), pH, and 4-NP concentrations (mg/L).

Experiment

Materials

Raw kaolin clay was obtained from Hadiya, Ethiopia. Iron (III) chloride hexahydrate ($FeCl_3{\cdot}6H_2O$), iron (II) sulfate heptahydrate ($FeSO_4{\cdot}7H_2O$), concentrated sulfuric acid (H_2SO_4, 18.4 mol/L), hydrochloric acid (HCl, 12 mol/L), ammonia (NH_3, 13.4 mol/L), and hydrogen peroxide (H_2O_2, 9.79 mol/L) were purchased from Merck, India, and used as received. Double distilled water was used throughout the whole experimental process.

Acid activation of kaolin

Kaolin was activated by H_2SO_4 based on a protocol reported in previous work.[34,35] Particularly, the raw kaolin sample was purified by washing with distilled water 3 times followed by drying in an oven at 105°C for 3 hours. The dried sample was crushed to obtain a fine powder that was able to pass through a 63-μm mesh size sieve. The sieved sample was further washed with distilled water and the dispersed clay separated by centrifugation. The washing process was continued 4 times to obtain pure kaolin. The wetted samples were dried in an oven at 105°C for 3 hours. Then, the powdered kaolin (6 g) was mixed with 180 mL of sulfuric acid (0.5 mol/L) and refluxed for 12 hours at 70°C for activation. The slurry was washed with distilled water 3 times till the supernatant became neutral with no trace amount of sulfate ion present. The slurry was separated and dried in an oven at 105°C for 3 hours. The final powder product (<63 μm size) is designated as activated kaolin (AK).

Synthesis of magnetite nanoparticles

The facile coprecipitation technique was used to synthesize Fe_3O_4 NPs. In particular, aqueous solutions of ferric and ferrous salts were mixed together in a molar ratio of 2:1, respectively. The mixture was heated with continuous stirring under reflux setup, and then NH_3 was added drop by drop to adjust the pH of the solution to 10. The solution was heated at 70°C for 45 minutes. Finally, the product was washed 3 times with distilled water to remove excess ammonium and dried under vacuum.

Synthesis of AK-Fe_3O_4 composite

The magnetically separable AK-Fe_3O_4 composite was synthesized by in situ coprecipitation of Fe_3O_4 NPs onto AK. The solution of $FeCl_3{\cdot}6H_2O$ and $FeSO_4{\cdot}7H_2O$ in a 2:1 molar ratio, respectively, was added drop by drop to 100 mL of AK solution. The mass ratio of iron salts to AK was fixed at 2:1, 4:1, and 6:1, respectively. After 30 minutes of continuous stirring, the ammonia solution was added to adjust the pH to 10. Then, the solution was refluxed for 8 hours at 70°C. The dark brown precipitate was washed 3 times with distilled water and dried under vacuum.

Characterization techniques

The functional groups present on the synthesized materials were investigated by FTIR spectroscopy. The FTIR was recorded using the Perkin Elmer FT-IR (spectrum RX-I) spectrometer in the range 400 to 4000 cm^{-1} by mixing the samples with spectroscopy-grade KBr in 1:2 mass ratio. X-ray

Downloaded From: https://complete.bioone.org/journals/Air,-Soil-and-Water-Research on 28 Mar 2024
Terms of Use: https://complete.bioone.org/terms-of-use

diffraction patterns of samples were recorded using SHIMADZU XRD, excellent in the science of XRD (model number XRD-7000; Shimadzu, Kyoto, Japan), which was operated at 40 kV and 45 mA, with a Cu-Kα (λ = 1.54056 Å) radiation. Scanning electron microscopy studies of the morphology of AK-Fe_3O_4 were analyzed by microstructure analysis with a Nova NanoSEM analyzer operated at an accelerating voltage of 10 keV. The samples were degassed at 150°C under vacuum. The magnetic property AK-Fe_3O_4 was investigated using a VSM (Lakeshore 665; Lake Shore Cryotronics, Inc., Westerville, OH, USA) at room temperature. The pH of point of zero charge (pH_{PZC}) of AK-Fe_3O_4 was determined to know the surface charge of AK-magnetite nanoparticles. For this purpose, 50 mL of sodium chloride (NaCl) solution was placed in a 100-mL Erlenmeyer flask. The pH was then adjusted to successive initial values between 3 and 9 using either sodium hydroxide or hydrogen chloride (0.1 mol/L), and 0.15 g of adsorbent (AK-Fe_3O_4) was added to the solution. After a contact time of 24 hours, the final pH was measured and plotted against the final pH. The pH at which the curve crosses the line pH (final-initial) is taken as pH_{PZC}.

RSM-BBD optimization of the Fenton-like degradation variables

The Fenton-like degradation of 4-NP was carried out in a batch reactor at varying concentrations of 4-NP. Specifically, 50 mg of the Fenton catalyst was added to 50 mL of 4-NP solution (10-30 mg/L) and stirred continuously. After adding the oxidation catalyst, 0.5 mL of H_2O_2 (9.79 mol/L) was added to the solution, which is considered as the initial (time $t = 0$) for the reaction. The pH of the solution was adjusted using NaOH (0.1 mol/L) and HCl (0.1 mol/L). The degradation (%) of 4-NP was analyzed by measuring the absorbance at $\lambda_{max} = 400$ nm using an ultraviolet-visible spectroscopy. The RSM-BBD optimization of 4-NP degradation mainly focused on 3 independent variables: pH, contact time (minutes), and concentration of 4-NP (mg/L). These 3 variables are selected because catalysis processes are highly dependent on them. The other remaining variables including 0.5 mL of 9.79 mol/L H_2O_2 (97.9 mmol/L), 50 mg of catalyst dose in 50 mL solution (1 mg/mL), and room temperature (298 K) were fixed throughout the whole reaction process. Design Expert 11 software program was used to compute the statistical analysis. The experimental levels of factors used for RSM-BBD are given in Table 1.

Table 1. The experimental levels of factors used for RSM-BBD.

FACTORS	LEVELS		
	LOW (−1.000)	CENTER (0.000)	HIGH (1.000)
A = x_1: time (min)	10	50	90
B = x_2: pH	3	5.5	8
C = x_3: 4-nitrophenol (mg/L)	10	20	30

Abbreviation: RSM-BBD, response surface methodology coupled with Box-Behnken design.

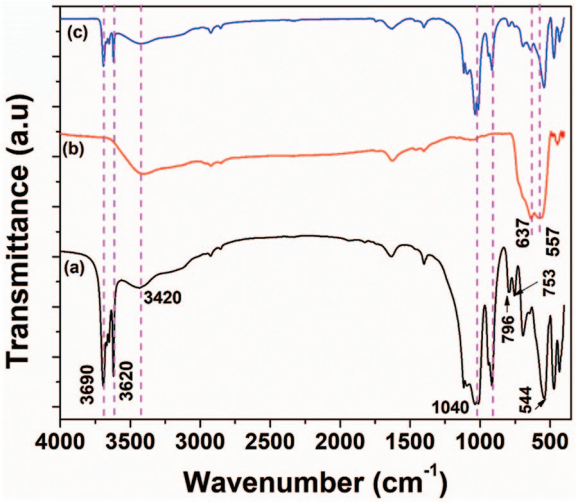


Figure 1. Fourier transform infrared spectra of (A) activated kaolin (AK), (B) Fe_3O_4, and (C) AK-Fe_3O_4 composites.

Results and Discussion

Characterizations

FITR analysis. Figure 1 shows the FTIR spectra of AK, Fe_3O_4 NPs, and AK-Fe_3O_4 composite. Activated kaolin (Figure 1A) shows 2 clearly identifiable bands at 3690 and 3620 cm^{-1}. The peak at 3690 cm^{-1} is due to stretching vibrations of surface hydroxyl groups, whereas the other peak at 3620 cm^{-1} is ascribed to the vibrations of inner hydroxyl groups.[36] The absorption bands observed at 3420 cm^{-1} could be assigned to the OH vibrational mode of water. The band associated with Si-O deformation is detailed to be 1040 cm^{-1}.[37] The band at 796 cm^{-1} is assigned to the Si-O-Si symmetric stretch.[38] Besides, a strong peak at 544 cm^{-1} indicates the presence of Si-O-Al stretching vibrations.[39] Figure 1B shows the FTIR spectrum obtained from pure magnetite nanoparticles. The 2 intense strong peaks observed at 557 and 637 cm^{-1} are attributed to the symmetric stretching vibration mode associated with Fe-O bond in the crystalline lattice of Fe_3O_4.[40] The FTIR spectrum of AK-Fe_3O_4 composite (Figure 1C) shows the peak due to both AK and Fe_3O_4 NPs, which implies the formation of the composite. But the intensity of inner and outer hydroxyl (OH) of kaolin becomes weak in the composite, indicating interruption of the kaolin structure.[41] This weak intensity is due to the exchange of Al^{3+} of kaolin structure with Fe^{3+} from Fe_3O_4.[41]

XRD analysis. The powder XRD analysis identified the unknown clay to be kaolin, and crystallite size and lattice cell parameters of Fe_3O_4 NPs, AK, and AK-Fe_3O_4

Downloaded From: https://complete.bioone.org/journals/Air,-Soil-and-Water-Research on 28 Mar 2024
Terms of Use: https://complete.bioone.org/terms-of-use

composites. The raw clay obtained from Hadiya, Ethiopia, was found to be kaolin. As shown in Figure 2A, raw kaolin is exactly matched with kaolinite $Al_2H_4O_9Si_2$ (COD: 00-900-9230).[42] The raw kaolin after chemical activation did not show a significant change in the XRD pattern compared with the raw kaolin (Supplemental Figure 1). Figure 2B shows the formation of spinel-type Fe_3O_4 NPs with 14 nm average crystallite size (*D*) calculated using Scherrer formula (equation (1)).[43] The characteristic plans are observed at (220), (311), (400), (422), (511), (440), and (553), which are in agreement with the inverse cubic spinel structure of Fe_3O_4 (JCPDS card no. 85-1436, space group Fd3m). Figure 2C presents the XRD patterns of the AK-Fe_3O_4 composite. The characteristic peaks due to Fe_3O_4 and AK were observed concurrently in the AK-Fe_3O_4 composite. The analysis illustrates that inverse spinel Fe_3O_4 NPs were successfully precipitated with activated clay to form the AK-Fe_3O_4 composite.[44] Besides, the average crystallite size of Fe_3O_4 NPs was found to be 11 nm which is less than naked Fe_3O_4 NPs. Moreover, the intercalation of Fe_3O_4 into AK layer is plausibly investigated by calculating the interplanar distance (*d*) before and after Fe_3O_4 NP treatment. As shown in Supplemental Figure 2, 2θ and *d* values at (100) of AK are different before and after Fe_3O_4 NP treatment. The shift of diffraction angle from 2θ = 12.3776° to 2θ = 12.0862° and expanding of the *d* value from 7.14531 to 7.31692 Å are attributed to the intercalation of Fe_3O_4 to the AK layer:[45]

$$D = \frac{0.9\lambda}{\beta\cos\theta} \quad (1)$$

where λ is the wavelength of the x-ray source (λ = 0.15418 nm), β is the peak width of the diffraction peak profile at half maximum height resulting from small crystallite size in radians, and θ is the Bragg angle.

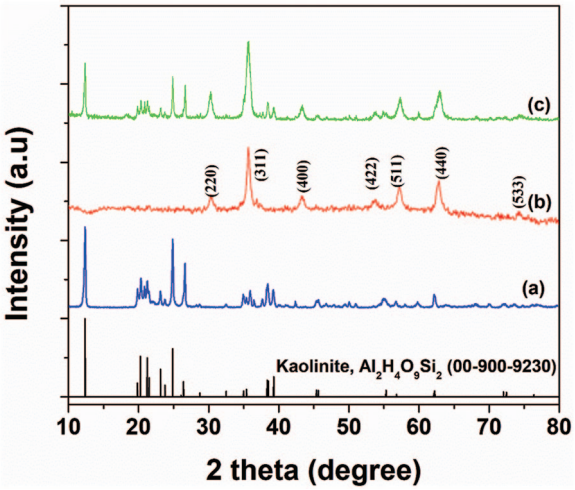


Figure 2. The powder x-ray diffraction patterns of (A) activated kaolin (AK), (B) Fe_3O_4, and (C) AK-Fe_3O_4 composite.

SEM, VSM, and pH_{PZC} analyses. The rough texture of the AK-Fe_3O_4 composite was investigated by the SEM image (Figure 3A). AK-Fe_3O_4 due to the formation of an infinite number of pores on the surface increases the surface area for adsorption of 4-NP. The magnetization value of naked Fe_3O_4 and AK-Fe_3O_4 was recorded at 300 K using VSM to investigate their magnetic nature. As shown in Figure 3B, both naked Fe_3O_4 and AK-Fe_3O_4 composites show superparamagnetic nature with zero remanence and coercivity. The saturation magnetization (MS) was found to be 57 and 25 emu/g for the naked Fe_3O_4 NPs and AK-Fe_3O_4 composite, respectively. In this sense, in the AK-Fe_3O_4 composite, the non-magnetic kaolin is responsible for weakening the magnetization value. Besides, those magnetization values are significantly lower than bulk Fe_3O_4 (MS ~82 emu/g).[46] The plot of ΔpH versus initial pH of the solution of AK-Fe_3O_4 is presented in Supplemental Figure 3. It is revealed that the AK-Fe_3O_4 composite shows a positive charge below pH_{PZC} = 6 and shows a negative charge as the pH increases.

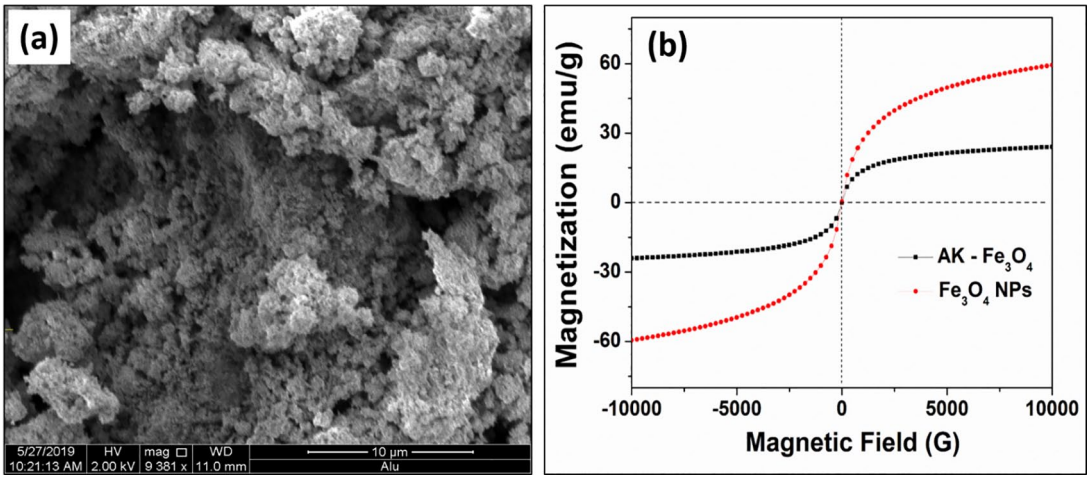


Figure 3. (A) Representative scanning electron microscopy image and (B) vibrating sample magnetometer curve of AK-Fe_3O_4 composite. AK indicates activated kaolin; NPs, nanoparticles.

Downloaded From: https://complete.bioone.org/journals/Air,-Soil-and-Water-Research on 28 Mar 2024
Terms of Use: https://complete.bioone.org/terms-of-use

Table 2. The RSM-BBD design matrix of the 3 variables with coded and real values, and response with actual and predicted values.

	CODED VALUES			REAL VALUES			RESPONSE	
	A	*B*	*C*	*A*	*B*	*C*	ACTUAL	PREDICTED
1	0.000	0.000	0.000	50	5.5	20	81	81.60
2	0.000	0.000	0.000	50	5.5	20	81	81.60
3	0.000	1.000	–1.000	50	8	10	65	65.50
4	0.000	0.000	0.000	50	5.5	20	79	81.60
5	0.000	0.000	0.000	50	5.5	20	82	81.60
6	–1.000	0.000	–1.000	10	5.5	10	47	47.63
7	0.000	–1.000	1.000	50	3	30	74	73.50
8	0.000	0.000	0.000	50	5.5	20	85	81.60
9	–1.000	0.000	1.000	10	5.5	30	23	23.88
10	1.000	1.000	0.000	90	8	20	71	71.38
11	1.000	0.000	1.000	90	5.5	30	74	73.38
12	1.000	0.000	–1.000	90	5.5	10	83	82.13
13	–1.000	–1.000	0.000	10	3	20	54	53.63
14	1.000	–1.000	0.000	90	3	20	93	94.13
15	–1.000	1.000	0.000	10	8	20	29	27.88
16	0.000	1.000	1.000	50	8	30	46	46.25
17	0.000	–1.000	–1.000	50	3	10	87	86.75

Abbreviation: RSM-BBD, response surface methodology coupled with Box-Behnken design.

Optimization of 4-NP degradation using RSM-BBD

During catalysis reaction, optimizations of the process variables using statistical approaches are crucial for the economic utilization of time and resources. Moreover, the statistical analysis gives a clear understanding of the reaction process and minimizes the experimental errors. Herein, the RSM-BBD approach was applied to optimize the Fenton-like degradation of 4-NP using AK-Fe_3O_4 composite. Box-Behnken design is a second-order design (equation (2)) based on 3-level factorial designs.[47] The complete BBD matrix for the 3 independent variables (contact time (*A*), pH (*B*), and 4-NP concentration (*C*)) and the response of both coded and real values are presented in Table 2:

$$Y = b_0 + \sum_{i=1}^{n} b_i X_i + \sum_{i=1}^{n-1} \sum_{j=i+1}^{n} b_{ij} X_i X_j \quad (2)$$

where Y is the predicted response (degradation, %) of 4-NP; b is a constant; and b_i, b_{ii}, and b_{ij} refer to the linear, quadratic, and interaction coefficients, respectively. X_i and X_j are lists of the coded values of factors.

The final equation (equation (3)) generated from 4-NP degradation using H_2O_2-AK-Fe_3O_4 based on BBD was found to be well fitted to the quadratic model:

$$\begin{aligned} \text{Degradation } (y) = {} & 81.6 + 21A - 12.13B - 8.13C \\ & + 0.75AB + 3.75AC - 1.50BC \\ & - 15.55A^2 - 4.30B^2 - 9.30C^2 \end{aligned} \quad (3)$$

Equation (3) shows how the 3 factors in a quadratic or interactive model affect the 4-NP degradation using the AK-Fe_3O_4 composite. As shown in equation (3), those with negative coefficients affect 4-NP degradation inversely, whereas those with positive coefficients enhance the degradation of 4-NP. Moreover, the adequacy of the quadratic model to sufficiently explain the 4-NP degradation process is validated via statistical parameters such as R^2 and analysis of variance (ANOVA). The detailed ANOVA results of 4-NP degradation using AK-Fe_3O_4 are presented in Table 3. As shown in Table 3, R^2 (0.9964) is much closer to unity, which implies that the data are well fitted to the quadratic model. In particular, 99.64% of the Fenton-like degradation of 4-NP can be described by the proposed quadratic model (equation (3)). Besides, Figure 4 shows that the predicted R^2 (0.9823) has a reasonable agreement with adjusted R^2 (0.9917), that is, the difference is less than 0.2. It is affirmed that the model can sufficiently explain the relationship between factors and 4-NP degradation (%).

The ANOVA (Table 3) of the model F value is 214.69, which implies that the quadratic model is significant and there

Downloaded From: https://complete.bioone.org/journals/Air,-Soil-and-Water-Research on 28 Mar 2024
Terms of Use: https://complete.bioone.org/terms-of-use

Table 3. The analysis of variance of 4-nitrophenol degradation based on quadratic model.

SOURCE	SUM OF SQUARES	DF	MEAN SQUARE	*F* VALUE	*P* VALUE	FIT STATISTICS
Model	6886.81	9	765.20	214.69	<.0001	SD = 1.89
Residual	24.95	7	3.56	–	–	CV(%) = 2.78
Lack of fit	5.75	3	1.92	0.3993	.7617	R^2 = 0.9964 Predicted R^2 = 0.9823
Pure error	19.20	4	4.80	–	–	Adjusted R^2 = 0.9917
TERMS	**COEFFICIENTS**		**SE COEFFICIENTS**	**MEAN SQUARE**	***F* VALUE**	***P* VALUE**
Constant	+81.60					
A	+21.00		0.3536	3528.00	989.82	<.0001
B	–12.13		0.3536	1176.12	329.97	<.0001
C	–8.13		0.3536	528.13	148.17	<.0001
AB	+0.7500		0.5000	2.25	0.6313	.4530
AC	+3.75		0.5000	56.25	15.78	.0054
BC	–1.50		0.5000	9.00	2.53	.1561
A^2	–15.55		0.4873	1018.12	285.64	<.0001
B^2	–4.30		0.4873	77.85	21.84	.0023
C^2	–9.30		0.4873	364.17	102.17	<.0001

Abbreviation: CV, coefficient of variation.

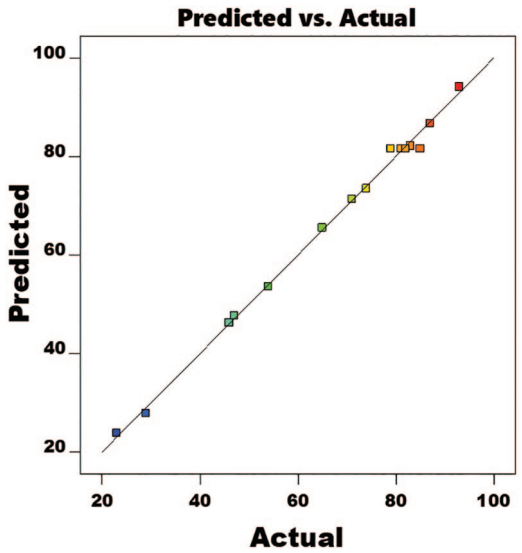


Figure 4. The comparison of actual (experimental) and model prediction values of 4-nitrophenol degradation (%).

is only a 0.01% chance that an *F* value this large could occur due to noise. The *P* value (<.0001) of the model also shows the significance of the model. Moreover, the significance of the model parameters is also validated by *P* values. The *P* value less than .05 (5%) indicates the model terms are significant. Herein, all the linear (*A*, *B*, and *C*), quadratic (A^2, B^2, and C^2), and interaction (*AC*) terms are significant, whereas model terms greater than 0.1 are not significant; therefore, the *AB* and *BC* interaction model terms are not insignificant.

The lack of fit (*F* = 0.40) from ANOVA (Table 3) implies that the lack of fit is not significant compared with the pure error. There is a 76.17% chance that a lack of fit *F* value this large could occur due to noise. This implies that the Fenton-like degradation of 4-NP is well explained by our quadratic model with a 95% confidence level.

The 2-dimensional (2D) and 3-dimensional (3D) surface plots of the response as a function of process variables are useful for a clear understanding of the reaction process. The 2D-3D plots (Figure 5) show the 4-NP degradation (%) with varying contact time, pH, and 4-NP concentrations. The degradation (%) of 4-NP differs with varying interaction variables and is found to be maximum with AB interaction terms than with AC and BC at a fixed 1 mg/mL concentration of AK-Fe_3O_4. As shown in Figure 5A, the AB interaction optimized at a fixed 4-NP concentration (20 mg/L) is the most important interaction parameter in predicting the maximum degradation of 4-NP. Hence, the optimum 4-NP degradation in 50 mL solution was found to be 96.01% ± 1.89% using 1 mg/mL of AK-Fe_3O_4, 20 mg/L of 4-NP, 97.9 mmol/L of

Downloaded From: https://complete.bioone.org/journals/Air,-Soil-and-Water-Research on 28 Mar 2024
Terms of Use: https://complete.bioone.org/terms-of-use

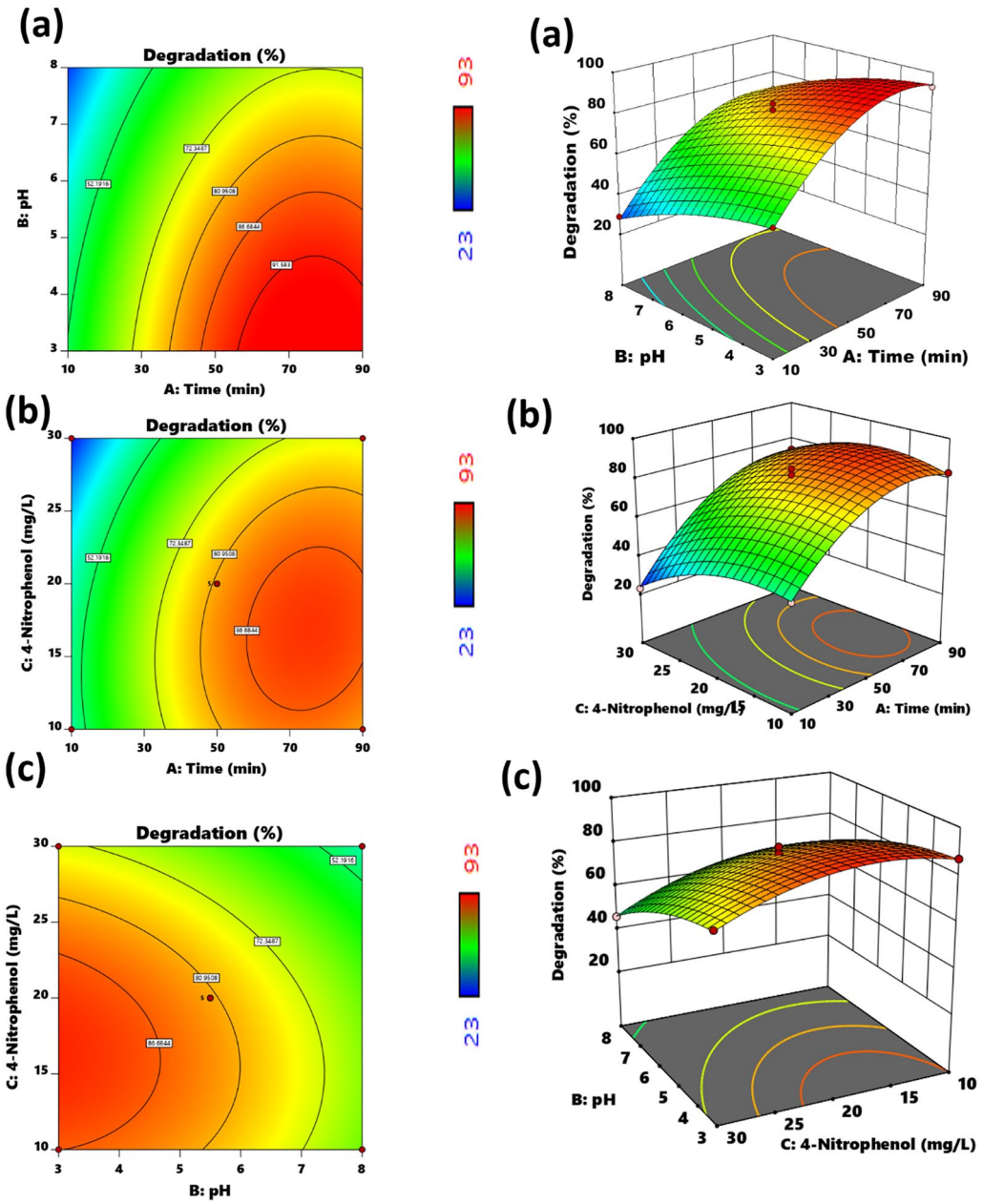


Figure 5. The 2-dimensional and 3-dimensional surface plots of the effect of (A) contact time and pH, (B) initial 4-NP concentration and contact time, and (C) 4-NP initial concentration and pH of solution on the degradation (%) efficiency of 4-NP by AK-Fe3O4 composite. AK indicates activated kaolin; 4-NP, 4-nitrophenol.

H_2O_2, and pH of 3 at the end of 75 minutes of reaction time. Moreover, the RSM-BBD optimization with other scenarios gives maximum degradation of 4-NP, and based on considering the available resource it is possible to adapt different combinations of contact time, pH, and 4-NP concentration.

In general, the numerical optimization of the desired goal is expected to maximize, minimize, target, be within the range, and be none of the responses and adjust to a precise value for the factors.[48] Herein, the numerical optimization found a point that maximizes the desirability function in 4-NP degradation. For example, the criteria set for the 3 factors in the range including contact time (10-90 minutes), pH of the solution (3-8), and initial 4-NP concentration (10-30 mg/L) and 96.08% maximum degradation of 4-NP were found to be the maximum desirability. Figure 6 shows ramp desirability that was generated from 100 optimum points via numerical optimization.

Mechanism and kinetics of 4-NP degradation

Supplemental Figure 4(a) shows the removal of 4-NP with and without H_2O_2. AK, Fe_3O_4, AK-Fe_3O_4, and H_2O_2 show very less removal of 4-NP, whereas AK-Fe_3O_4 composite in combination with H_2O_2 shows a significant degradation of 4-NP. This is attributed to the removal of 4-NP, which was predominantly through Fenton-like degradation of 4-NP. Moreover,

Downloaded From: https://complete.bioone.org/journals/Air,-Soil-and-Water-Research on 28 Mar 2024
Terms of Use: https://complete.bioone.org/terms-of-use

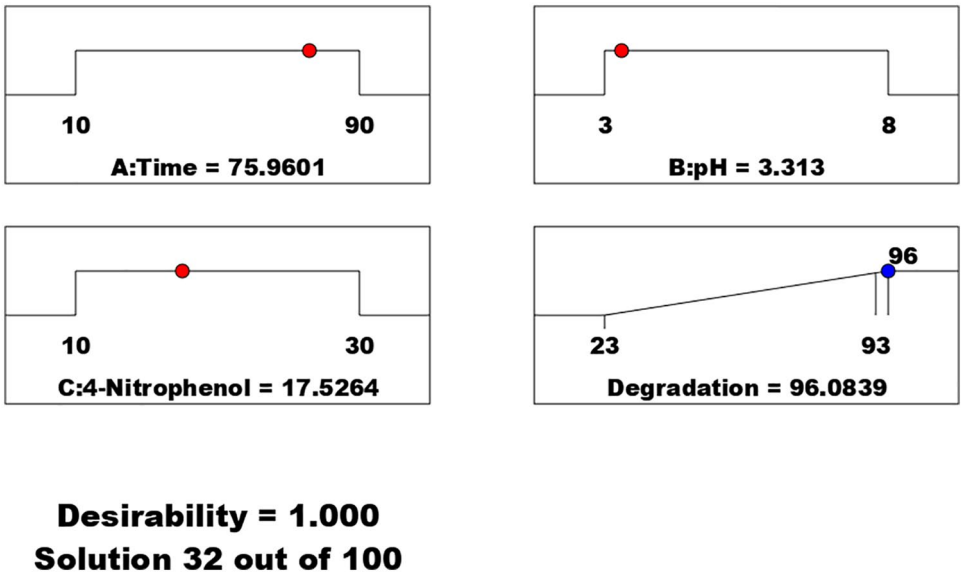


Figure 6. The desirability ramp for optimization of 3 factors (contact time, pH solution, and 4-NP concentration) for the maximum degradation (%) of 4-NP using AK-Fe_3O_4 composite. AK indicates activated kaolin; 4-NP, 4-nitrophenol.

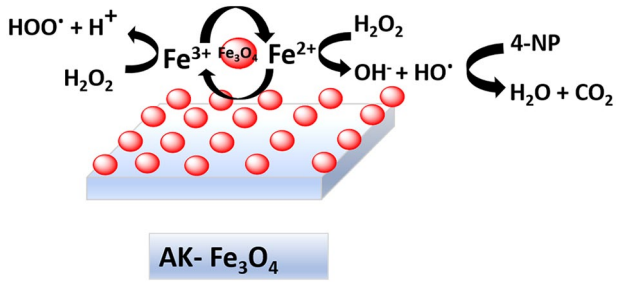


Figure 7. The plausible Fenton-like degradation of 4-NP using AK-Fe_3O_4 composite as a catalyst for the activation of H_2O_2. AK indicates activated kaolin; 4-NP, 4-nitrophenol.

Supplemental Figure 4(b) shows the comparative degradation efficiency of AK/H_2O_2, Fe_3O_4/H_2O_2, and AK-Fe_3O_4/H_2O_2. Fe_3O_4/H_2O_2 and AK-Fe_3O_4/H_2O_2 due to the presence of Fe_3O_4, which activates H_2O_2, show greater degradation efficiency than AK/H_2O_2.[20] For Fenton-like reaction on the iron-based heterogeneous catalyst, the activation of H_2O_2 using $Fe^{2}+$ and $Fe^{3}+$ proceeds via adsorption of H_2O_2 on the catalyst surface, which in turn depends on the surface area of the catalyst.[49] Fe_3O_4 nanoparticles show a strong affinity toward H_2O_2, which facilitates the formation of active oxidizing agents ($HO^{\bullet}$ and $HO_2^{\bullet}$).[25,49] The plausible mechanism for the degradation of 4-NP using the AK-Fe_3O_4/H_2O_2 system can be suggested as shown in Figure 7. Hence, H_2O_2 is initially adsorbed on the AK-Fe_3O_4 composite where it is activated by Fe_3O_4 for the formation of $HO^{\bullet}$ and $HOO^{\bullet}$. $HO^{\bullet}$ is a powerful oxidant that can mineralize 4-NP into H_2O and CO_2.

The kinetics of the Fenton-like degradation of the 4-NP can be investigated using the pseudo-first-order equation (equation (4)):[29]

$$\ln\left(\frac{C_t}{C_o}\right) = -kt \quad (4)$$

where C_o and C_t are the initial and final concentrations at time "t" of 4-NP. Therefore, a plot of $\ln(C_t/C_o)$ with respect to reaction time gives a straight line whose slope is k (Supplemental Figure 4(c)). The kinetic analysis was performed by varying the initial concentrations of 4-NP while maintaining others constant. As shown in Supplemental Figure 4(d), the rate constant (k) decreases with an increase in 4-NP concentrations. This implies that 4-NP degradation is relatively fast at low concentration. Moreover, Supplemental Table 1 shows the comparison of AK-Fe_3O_4 with other catalysts used for 4-NP Fenton-like degradations. AK-Fe_3O_4 shows faster 4-NP degradation efficiency than others that are working at room temperature (298 K).

Reusability and stability of AK-Fe_3O_4

Reusability and stability are very important criteria for evaluating the practical application of catalysts. Successive cycles of the Fenton degradation were carried out to evaluate the stability and reusability of our catalyst under the same reaction conditions. The optimum condition of degradation parameters in 50 mL solution such as 1 mg/mL of AK-Fe_3O_4, 20 mg/L of 4-NP, 97.9 mmol/L of H_2O_2, and pH of 3 at the end of 75 minutes of reaction time was used to investigate the stability and reusability of the catalyst. After each successive cycle, the AK-Fe_3O_4 was collected by centrifugation, washed at least 3 times, and dried in the oven at 100°C for 12 hours.[50] As shown in Figure 8, the catalyst could be successfully reused for 5 successive degradation cycles with more than 90% degradation efficiency, indicating that the AK-Fe_3O_4 Fenton-like catalyst is stable. Moreover, the stability of the AK-Fe_3O_4 before and after 5 times use was examined by XRD. As can be seen from Figure 9, the XRD patterns of AK-Fe_3O_4 do not change before and after degradation. This implies the stability of the catalyst

Downloaded From: https://complete.bioone.org/journals/Air,-Soil-and-Water-Research on 28 Mar 2024
Terms of Use: https://complete.bioone.org/terms-of-use

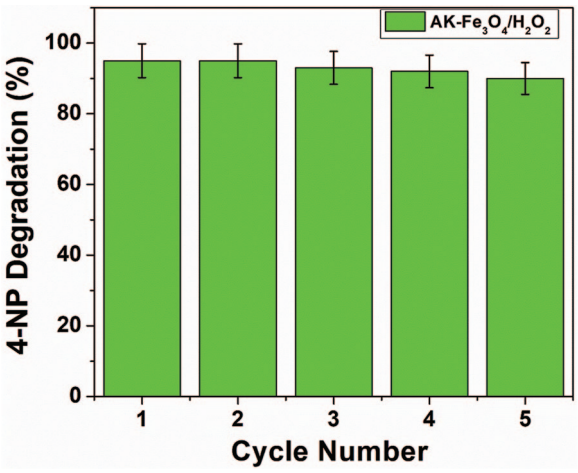


Figure 8. The reusability of AK-Fe_3O_4/H_2O_2 for the degradation (%) of 4-NP in 50 mL solution (1 mg/mL of AK-Fe_3O_4, 20 mg/L of 4-NP, 97.9 mmol/L of H_2O_2, pH of 3; contact time, 75 minutes). Error bar represents 5% error. AK indicates activated kaolin; 4-NP, 4-nitrophenol.

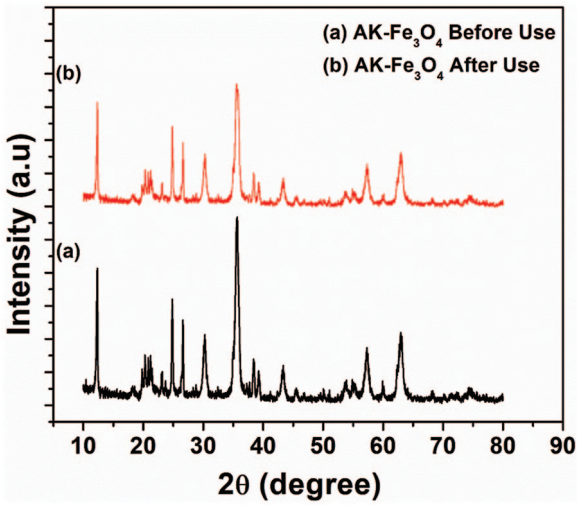


Figure 9. The x-ray diffraction patterns of AK-Fe_3O_4 (A) before and (B) after Fenton-like degradation of 4-NP. AK indicates activated kaolin; 4-NP, 4-nitrophenol.

crystal structure after use.[51] But the peak intensity decreased after use, which is possibly due to catalyst loss during recovery.

Conclusion

In conclusion, Fe_3O_4-modified AK was successfully prepared using a facile in situ coprecipitation of Fe_3O_4 in the presence of kaolin. The crystal structure, phase formation, and surface morphology were characterized by XRD, FTIR, SEM, and VSM. The AK-Fe_3O_4 composite is effective for Fenton-like degradation of 4-NP. The most important 4-NP degradation parameters (such as contact time, concentrations of 4-NP, and pH) were optimized using RSM-BBD. A 3-level quadratic model can effectively show the interaction of parameters. This was validated by both regression ($R^2 = 0.9964$ and adjusted $R^2 = 0.9917$) and ANOVA ($P < .0001$) analyses. Based on RSM-BBD, the optimum 4-NP degradation in 50 mL solution was found to be 96.01% ± 1.89% with the use of 1 mg/mL of AK-Fe_3O_4, 20 mg/L of 4-NP, 97.9 mmol/L of H_2O_2 and pH of 3 at the end of 75 minutes of reaction time. Moreover, the RSM-BBD can suggest other optimization scenarios that give maximum degradation of 4-NP based on the available resource. Thus, the AK-Fe_3O_4 composite and optimization using RSM-BBD can be applied for the Fenton-like degradation of water pollutants. Moreover, the catalyst shows good recyclability and stability after 5 successive degradations of 4-NP.

Acknowledgements

The authors acknowledge Debre Berhan University for supporting the work. The authors also acknowledge Adama Science and Technology University for recording the x-ray diffraction samples.

Author Contributions

NB designed the study, contributed to data interpretation, and edited the manuscript. RF helped with the experiment and wrote the manuscript. AA helped with the experiment and contributed to data interpretation. All authors read and approved the final manuscript.

ORCID iD

Neway Belachew https://orcid.org/0000-0003-1445-7039

Supplemental Material

Supplemental material for this article is available online.

REFERENCES

1. Raja ASM, Arputharaj A, Saxena S, Patil PG. Water requirement and sustainability of textile processing industries. In: Muthu SS, ed. *Water in Textiles and Fashion*. Oxford, UK: Elsevier; 2019:155-173.
2. Ahmad A, Mohd-Setapar SH, Chuong CS, et al. Recent advances in new generation dye removal technologies: novel search for approaches to reprocess wastewater. *RSC Adv*. 2015;5:30801-30818.
3. Lellis B, Fávaro-Polonio CZ, Pamphile JA, Polonio JC. Effects of textile dyes on health and the environment and bioremediation potential of living organisms. *Biotechnol Res Innov*. 2019;3:275-290.
4. Belachew N, Meshesha DS, Basavaiah K. Green syntheses of silver nanoparticle decorated reduced graphene oxide using l-methionine as a reducing and stabilizing agent for enhanced catalytic hydrogenation of 4-nitrophenol and antibacterial activity. *RSC Adv*. 2019;9:39264-39271.
5. Nehru R, Gopi PK, Chen S-M. Enhanced sensing of hazardous 4-nitrophenol by a graphene oxide–TiO_2 composite: environmental pollutant monitoring applications. *New J Chem*. 2020;44:4590-4603.
6. Lichtveld MY, Rodenbeck SE, Lybarger JA. The findings of the Agency for Toxic Substances and Disease Registry Medical Waste Tracking Act report. *Environ Health Perspect*. 1992;98:243-250.
7. Alam U, Kumar S, Bahnemann D, Koch J, Tegenkamp C, Muneer M. Harvesting visible light with MoO nanorods modified by Fe(iii) nanoclusters for effective photocatalytic degradation of organic pollutants. *Phys Chem Chem Phys*. 2018;20:4538-4545.
8. Guo K, Gao B, Tian X, et al. Synthesis of polyaluminium chloride/papermaking sludge-based organic polymer composites for removal of disperse yellow and reactive blue by flocculation. *Chemosphere*. 2019;231:337-348.
9. Wawrzkiewicz M. Anion exchange resins as effective sorbents for acidic dye removal from aqueous solutions and wastewaters. *Solvent Extr Ion Exc*. 2012;30:507-523.
10. Song Y, Seo JY, Kim H, Beak K-Y. Structural control of cellulose nanofibrous composite membrane with metal organic framework (ZIF-8) for highly selective removal of cationic dye. *Carbohydr Polym*. 2019;222:115018.

Downloaded From: https://complete.bioone.org/journals/Air,-Soil-and-Water-Research on 28 Mar 2024
Terms of Use: https://complete.bioone.org/terms-of-use

11. Belachew N, Rama Devi D, Basavaiah K. Facile green synthesis of l-methionine capped magnetite nanoparticles for adsorption of pollutant Rhodamine B. *J Mol Liq*. 2016;224:713-720.
12. Sun S-P, Lemley AT. p-Nitrophenol degradation by a heterogeneous Fenton-like reaction on nano-magnetite: process optimization, kinetics, and degradation pathways. *J Mol Catal A: Chem*. 2011;349:71-79.
13. Zhao B, Mele G, Pio I, Li J, Palmisano L, Vasapollo G. Degradation of 4-nitrophenol (4-NP) using Fe–TiO_2 as a heterogeneous photo-Fenton catalyst. *J Hazard Mater*. 2010;176:569-574.
14. Zhang M-H, Dong H, Zhao L, Wang D-X, Meng D. A review on Fenton process for organic wastewater treatment based on optimization perspective. *Sci Total Environ*. 2019;670:110-121.
15. Babuponnusami A, Muthukumar K. A review on Fenton and improvements to the Fenton process for wastewater treatment. *J Environ Chem Eng*. 2014;2:557-572.
16. Jain A, Kotwal M, Khan S. Greener and expedient approach for the wastewater treatment by Fenton and photo-Fenton processes: a review. *AJCPS*. 2016;1:1.
17. Wu J, Wang X, Kang H, Zhang J, Yang C. $CuFe_2O_4$ as heterogeneous catalyst in degradation of p-nitrophenol with photoelectron-Fenton-like process. *Int J Environ Stud*. 2014;71:534-545.
18. Li X, Huang Y, Li C, Shen J, Deng Y. Degradation of pCNB by Fenton like process using α-FeOOH. *Chem Eng*. 2015;260:28-36.
19. di Luca C, Massa P, Fenoglio R, Cabello FM. Improved Fe_2O_3/Al_2O_3as heterogeneous Fenton catalysts for the oxidation of phenol solutions in a continuous reactor. *J Chem Technol Biotechnol*. 2014;89:1121-1128.
20. Jia X, Chen X, Liu Y, Zhang B, Zhang H, Zhang Q. Hydrophilic Fe_3O_4 nanoparticles prepared by ferrocene as high-efficiency heterogeneous Fenton catalyst for the degradation of methyl orange. *Appl Organomet Chem*. 2019;33:e4826.
21. Belachew N, Rama Devi D, Basavaiah K. Green synthesis and characterisation of L-Serine capped magnetite nanoparticles for removal of Rhodamine B from contaminated water. *J Exp Nanosci*. 2017;12:114-128.
22. Popescu RC, Andronescu E, Vasile BS. Recent advances in magnetite nanoparticle functionalization for nanomedicine. *Nanomaterials (Basel)*. 2019;9:1791.
23. Zhang Y, Chen B, Zhang L, et al. Controlled assembly of Fe_3O_4 magnetic nanoparticles on graphene oxide. *Nanoscale*. 2011;3:1446-1450.
24. Chen L, Zhou CH, Fiore S, et al. Functional magnetic nanoparticle/clay mineral nanocomposites: preparation, magnetism and versatile applications. *Appl Clay Sci*. 2016;127-128:143-163.
25. Guo S, Zhang G, Wang J. Photo-Fenton degradation of rhodamine B using Fe_2O_3-Kaolin as heterogeneous catalyst: characterization, process optimization and mechanism. *J Colloid Interface Sci*. 2014;433:1-8.
26. Giri SK, Das NN, Pradhan GC. Magnetite powder and kaolinite derived from waste iron ore tailings for environmental applications. *Powder Technol*. 2011;214:513-518.
27. Janíková B, Tokarský J, Kutláková KM, Kormunda M, Neuwirthová L. Photoactive and non-hazardous kaolin/ZnO composites prepared by calcination of sodium zinc carbonate. *Applied Clay Science*. 2017;143:345-353.
28. Wang B, Ding H, Deng Y. Characterization of calcined kaolin/TiO_2 composite particle material prepared by mechano-chemical method. *J Wuhan Univ Technol-Mater Sci Ed*. 2010;25:765-769.
29. Ayodele OB, Hameed BH. Development of kaolinite supported ferric oxalate heterogeneous catalyst for degradation of 4-nitrophenol in photo-Fenton process. *Appl Clay Sci*. 2013;83-84:171-181.
30. Allouss D, Essamlali Y, Amadine O, Chakir A, Zahouily M. Response surface methodology for optimization of methylene blue adsorption onto carboxymethyl cellulose-based hydrogel beads: adsorption kinetics, isotherm, thermodynamics and reusability studies. *RSC Adv*. 2019;9:37858-37869.
31. Chellamboli C, Perumalsamy M. Application of response surface methodology for optimization of growth and lipids in Scenedesmus abundans using batch culture system. *RSC Adv*. 2014;4:22129-22140.
32. Belachew N, Bekele G. Synergy of magnetite intercalated bentonite for enhanced adsorption of congo red dye. *Silicon*. 2020;12:603-612.
33. Ferreira SLC, Bruns RE, Ferreira HS, et al. Box-Behnken design: an alternative for the optimization of analytical methods. *Anal Chim Acta*. 2007;597:179-186.
34. Al-Essa K. Activation of Jordanian bentonite by hydrochloric acid and its potential for olive mill wastewater enhanced treatment. *J Chem*. 2018;2018:1-10.
35. Belachew N, Hinsene H. Preparation of cationic surfactant-modified kaolin for enhanced adsorption of hexavalent chromium from aqueous solution. *Appl Water Sci*. 2020;10:38-45.
36. Tironi A, Trezza MA, Irassar EF, Scian AN. Thermal treatment of kaolin: effect on the pozzolanic activity. *Procedia Mat Sci*. 2012;1:343-350.
37. Hildebrando EA, Andrade CGB, da Rocha Junior CAF, Angélica RS, Valenzuela-Diaz FR, de Freitas Neves R. Synthesis and characterization of zeolite NaP using kaolin waste as a source of silicon and aluminum. *Mater Res*. 2014;17:174-179.
38. Ahangaran F, Hassanzadeh A, Nouri S. Surface modification of Fe_3O_4 @SiO_2 microsphere by silane coupling agent. *Int Nano Lett*. 2013;3:1-5.
39. Madejová J. FTIR techniques in clay mineral studies. *Vib Spectrosc*. 2003;31:1-10.
40. Cornell RM, Schwertmann U. *The Iron Oxides: Structure, Properties, Reactions, Occurrences and Uses*. Weinheim, Germany: John Wiley & Sons; 2006.
41. Magdy A, Fouad YO, Abdel-Aziz MH, Konsowa AH. Synthesis and characterization of Fe_3O_4 /kaolin magnetic nanocomposite and its application in wastewater treatment. *J Ind Eng Chem*. 2017;56:299-311.
42. Bish DL. Rietveld refinement of non-hydrogen atomic positions in kaolinite. *Clay Clay Miner*. 1989;37:289-296.
43. Patterson AL. The Scherrer formula for X-ray particle size determination. *Phys Rev*. 1939;56:978-982.
44. Rahman O, Mohapatra SC, Ahmad S. Fe_3O_4 inverse spinal super paramagnetic nanoparticles. *Mater Chem Phys*. 2012;132:196-202.
45. Qu H, He S, Su H. Efficient preparation of kaolinite/methanol intercalation composite by using a Soxhlet extractor. *Sci Rep*. 2019;9:8351.
46. Poth P. Corrosion books: the iron oxides —structure, properties, reactions, occurrences and uses. By: R. M. Cornell, U. Schwertmann. *Mater Corros*. 2004;55:704-704.
47. Cobas M, Sanromán MA, Pazos M. Box–Behnken methodology for Cr (VI) and leather dyes removal by an eco-friendly biosorbent: F. vesiculosus. *Bioresour Technol*. 2014;160:166-174.
48. Trinh H, Yusup S, Uemura Y. Optimization and kinetic study of ultrasonic assisted esterification process from rubber seed oil. *Bioresour Technol*. 2018;247:51-57.
49. Gonzalez-Olmos R, Holzer F-D, Kopinke F, Georgi A. Indications of the reactive species in a heterogeneous Fenton-like reaction using Fe-containing zeolites. *Appl Catal A: Gen*. 2011;398:44-53.
50. Yang X, Zhong H, Zhu Y, et al. Highly efficient reusable catalyst based on silicon nanowire arrays decorated with copper nanoparticles. *J Mater Chem A*. 2014;2:9040-9047.
51. Tian X, Liu Y, Chi W, et al. Catalytic degradation of phenol and p-nitrophenol using Fe_3O_4/MWCNT nanocomposites as heterogeneous Fenton-like catalyst. *Water Air Soil Pollut*. 2017;228:297-308.

Downloaded From: https://complete.bioone.org/journals/Air,-Soil-and-Water-Research on 28 Mar 2024
Terms of Use: https://complete.bioone.org/terms-of-use